Biogeosciences, 7, 2613–2624, 2010
www.biogeosciences.net/7/2613/2010/
doi:10.5194/bg-7-2613-2010

Biogeosciences

Ballast minerals and the sinking carbon flux in the ocean: carbon-specific respiration rates and sinking velocity of marine snow aggregates

M. H. Iversen[1,*] **and H. Ploug**[1,**]

[1]Alfred Wegener Institute for Polar and Marine Research, Am Handelshafen 12, 27570 Bremerhaven, Germany
[*]now at: Faculty of Geosciences and Marum, University of Bremen, Klagenfurter and Leobener Strasse, 28359 Bremen, Germany
[**]now at: Stockholm University, Dept. of Botany, Lilla Frescativägen 5, 10691 Stockholm, Sweden

Received: 7 April 2010 – Published in Biogeosciences Discuss.: 7 May 2010
Revised: 3 August 2010 – Accepted: 12 August 2010 – Published: 7 September 2010

Abstract. Recent observations have shown that fluxes of ballast minerals (calcium carbonate, opal, and lithogenic material) and organic carbon fluxes are closely correlated in the bathypelagic zones of the ocean. Hence it has been hypothesized that incorporation of biogenic minerals within marine aggregates could either protect the organic matter from decomposition and/or increase the sinking velocity via ballasting of the aggregates. Here we present the first combined data on size, sinking velocity, carbon-specific respiration rate, and composition measured directly in three aggregate types; *Emiliania huxleyi* aggregates (carbonate ballasted), *Skeletonema costatum* aggregates (opal ballasted), and aggregates made from a mix of both *E. huxleyi* and *S. costatum* (carbonate and opal ballasted). Overall average carbon-specific respiration rate was $\sim$0.13 d^{-1} and did not vary with aggregate type and size. Ballasting from carbonate resulted in 2- to 2.5-fold higher sinking velocities than those of aggregates ballasted by opal. We compiled literature data on carbon-specific respiration rate and sinking velocity measured in aggregates of different composition and sources. Compiled carbon-specific respiration rates (including this study) vary between 0.08 d^{-1} and 0.20 d^{-1}. Sinking velocity increases with increasing aggregate size within homogeneous sources of aggregates. When compared across different particle and aggregate sources, however, sinking velocity appeared to be independent of particle or aggregate size. The carbon-specific respiration rate per meter settled varied between 0.0002 m^{-1} and 0.0030 m^{-1}, and decreased with increasing aggregate size. It was lower for calcite ballasted aggregates as compared to that of similar sized opal ballasted aggregates.

Correspondence to: M. H. Iversen
(morten.iversen@uni-bremen.de)

1 Introduction

A large fraction of particulate organic matter occurs in the form of marine snow aggregates (>0.5 cm) composed of phytoplankton, detritus, inorganic mineral grains, and fecal pellets in the ocean (Alldredge and Silver, 1988). Formation and sinking of these aggregates drive the biological carbon pump via export and sedimentation of organic matter from the surface mixed layer to the deep ocean and sediments. The fraction of organic matter that leaves the upper mixed layer of the ocean is, among other factors, determined by the sinking velocity and microbial remineralization rate of these aggregates. Recent observations have shown that the fluxes of ballast minerals (calcium carbonate, opal, and lithogenic material) and the organic carbon fluxes are closely correlated in the bathypelagic zones of the ocean. This has lead to the hypothesis that organic carbon export is determined by the presence of ballast minerals within settling aggregates (Armstrong et al., 2002; Francois et al., 2002; Klaas and Archer, 2002). Hence, it has been proposed that organic carbon is better preserved in sinking particles due to increased aggregate density and sinking velocity when ballast minerals are present and/or via protection of the organic matter due to

quantitative association to ballast minerals (Armstrong et al., 2002; Francois et al., 2002; Klaas and Archer, 2002). Klaas and Archer (2002) observed that ∼83% of the global particulate organic carbon (POC) fluxes were associated with carbonate, and suggested that carbonate is a more efficient ballast mineral as compared to opal and terrigenous material. However, a study by De La Rocha et al. (2008) showed no evidence supporting calcium carbonate as a better carrier of organic matter than opal. Still, Klaas and Archer (2002) hypothesized that the higher density of calcium carbonate compared to that of opal and the higher abundance of calcium carbonate relative to terrigenous material might be the reason for the efficient ballasting by calcium carbonate. However, the direct effects of ballast minerals on sinking velocity and degradation rates in sinking aggregates are still unclear.

A recent study has demonstrated that copepod fecal pellets produced on a diet of diatoms or coccolithophorids show higher sinking velocities as compared to pellets produced on a nanoflagellate diet (Ploug et al., 2008b). Carbon-specific respiration rates in pellets, however, were similar and independent of mineral content. These results suggest that differences in mineral composition does not lead to differential protection of POC against microbial degradation, but the enhanced sinking velocities may result in up to 10-fold higher carbon preservation in pellets containing biogenic minerals as compared to that of pellets without biogenic minerals (Ploug et al., 2008b). However, the study by Ploug et al. (2008b) only investigated the degradation of labile organic matter and cannot exclude that mineral-associated organic matter is protected. Minerals seem to enhance the flocculation of phytoplankton aggregates (Engel et al., 2009a; Engel et al., 2009b) and may even act as a catalyst in aggregate formation (Lee et al., 2009). However, it has also been shown that incorporation of minerals can cause aggregates to fragment into smaller and denser aggregates (Passow and De La Rocha, 2006; Engel et al., 2009b). This can potentially lower the sinking velocity of the aggregated organic material due to the reduced aggregate sizes, and, thus, lower the total export of organic matter. Conversely, if the incorporation of minerals increases the aggregate density, its size-specific sinking velocity may also increase, which could potentially increase the carbon export. Therefore, there is still a need for better quantitative investigations of how the interactions between minerals and organic aggregates affect the degradation and sinking velocity of the aggregates and, hence, carbon sequestration in the ocean.

In this study, we investigated how the presence of opal, carbonate, or a mixture of opal and carbonate affects the sinking velocity and degradation of organic carbon in mm-large phytoplankton aggregates. The aggregates were formed in roller tanks from cultures of diatoms, coccolithophorids, or a mixture of both diatoms and coccolithophorids. Aggregate size, sinking velocity, and respiration rates were measured in a vertical flow system. An upward-directed flow balanced the aggregate sinking velocity, keeping the aggregate in suspension while the respiration was measured using an oxygen microsensor at the aggregate-water interface. Hence, respiration was measured under similar hydrodynamic conditions as those occurring at the aggregate water interface during sedimentation (Kiørboe et al., 2001). The composition of the same aggregate was analyzed after respiration measurements. This approach enabled us to test whether the apparent increased fluxes of ballasted marine snow aggregates occur due to increased density and sinking velocities of the aggregates or due to adsorptive protection of the organic matter to the biogenic minerals whereby the degradation rate is reduced. We compiled previous collected data on aggregate sinking velocities and degradation rates to identify general trends induced by the presence and/or absence of ballast minerals.

2 Materials and methods

2.1 Algae cultures

Cultures of the diatom *Skeletonema costatum* (North Sea) and the coccolithophorid *Emiliania huxleyi* (strain PML B92/11, North Sea) were grown for 13 days at 15 °C in 0.2 µm filtered seawater (salinity 32) enriched with nutrients according to f/2 medium (Guillard, 1975). The f/2 medium used for the diatoms was enriched with silicate at a molar ratio of silicate to nitrate of 1. The cultures were kept under a light:dark cycle (12:12 h) with light intensities of 150 µmol photons m^{-2} s^{-1}.

2.2 Aggregate formation

The algae cultures were incubated in 1.15 L Plexiglas cylinders (roller tanks, 14 cm diameter and 7.47 cm length) to form aggregates. Three different roller tank incubations were carried out in order to obtain aggregates formed with *Skeletonema costatum* (*S.c.*-inc), aggregates formed with *Emiliania huxleyi* (*E.h.*-inc), and aggregates formed with a mixture of *S. costatum* and *E. huxleyi* with 1:1 volume from the two cultures (mix-inc), respectively. The roller tanks were rotated on a rolling table at 3 rotations per minute (rpm) at 15 °C in constant dim light, ∼30 µmol photons m^{-2} s^{-1}.

2.3 Sinking velocity

Sinking velocity of single aggregates was measured in a vertical flow system (Ploug and Jørgensen, 1999; Ploug et al., 2010). Individual aggregates were gently transferred from the roller tanks to an open flow-through chamber using a wide bore pipette. The flow chamber was a 10 cm high Plexiglas tube (5 cm diameter) with a net extended in the middle. The net creates a relative uniform flow field across the upper chamber when a fluid flow is supplied from below (Ploug and Jørgensen, 1999). The flow was adjusted with a needle valve until the aggregate remained suspended at a distance of

one aggregate diameter above the net, whereby the aggregate sinking velocity was balanced by the upward-directed seawater flow velocity. The sinking velocity of an aggregate was calculated by dividing the flow rate by the cross-sectional area of the flow chamber. Triplicate measurements of sinking velocity were made for each aggregate.

2.4 Size measurements

The length of all three aggregate axes (x, y, and z direction) was measured in the flow system using a horizontal dissection microscope with a calibrated ocular. The aggregate volume was calculated by assuming an ellipsoid shape. For comparison with other aggregate shapes we calculated the equivalent spherical diameter (ESD) of each aggregate.

2.5 Oxygen measurements

Oxygen gradients at the aggregate-water interface were measured using a Clark-type oxygen microelectrode with a guard cathode (Revsbech, 1989) mounted in a micromanipulator and calibrated at air-saturation and at anoxic conditions. The electrode current was measured on a picoamperemeter (Unisense, PA2000) and read on a strip chart recorder (Kipp and Zonen) at high resolution ($2\,\mu M\,O_2\,cm^{-1}$). The tip diameter of the microsensor was 2 µm. The relative distance between the microelectrode tip and the aggregate surface was measured using a dissection microscope with a calibrated ocular micrometer. The 90% response time of the electrode was <1 s and the stirring sensitivity <0.3%. During O_2-measurements, the aggregates were suspended by an upward-directed flow that balanced the aggregate's sinking velocity in the same vertical net-jet flow system as used for estimating sinking velocities (Ploug and Jørgensen, 1999). The fluid motion and solute distribution in the vicinity of the aggregates under these experimental conditions are equivalent to those in the vicinity of an aggregate sinking through the water column at a velocity equal to the water flow velocity (Kiørboe et al., 2001). All measurements were done at steady state of the oxygen gradients. The water in the flow system was similar to the water in the roller tanks (0.2 µm filtered sea water at 15 °C with a salinity of 32).

2.5.1 Calculations of respiration rates

Respiration rates were calculated from the oxygen gradients measured at the aggregate-water interface at steady-state. The analytical solutions for oxygen distribution and diffusive fluxes at the aggregate-water interface were fitted to measured values by applying the solver routine of the spreadsheet program Excel version 97 (Microsoft) as previously described (Ploug et al., 1997). We used a temperature and salinity corrected oxygen diffusion coefficient of $1.71\times10^{-5}\,cm^2\,s^{-1}$ in the calculations (Broecker and Peng, 1974). The surface area of ellipsoids (Maas, 1994) was used to calculate total oxygen consumption. Oxygen consumption rate was converted to carbon respiration assuming a respiratory quotient of 1.2 mol O_2 to 1 mol CO_2, as also used in a previous study of O_2 respiration and POC degradation in diatom aggregates (Ploug and Grossart, 2000).

2.6 Aggregate dry weight and carbon content

The aggregate dry weight (DW) was determined by filtering single aggregates with known volumes onto pre-weighed 0.4-mm polycarbonate filters. Each filter contained one aggregate, which was gently washed with de-ionized water to remove salt and dried at 60 °C for 48 h before weighing on a Mettler Toledo (UMX 2) scale with a sensitivity of 0.1 µg.

The ratio of particulate organic carbon (POC) to DW was determined by filtering ~50 aggregates onto pre-weighed 25 mm GF/F filters. The filters were gently rinsed with de-ionized water, and dried at 40 °C for over 48 hours before being re-weighed on a Mettler Toledo UMX2 balance (sensitivity: 0.1 µg). POC content of the aggregates on each filter was measured on an EA mass spectrometer (ANCA-SL 20-20, Sercon Ltd. Crewe, UK) with a precision of ±0.7 µg C or 0.3%. For calcium carbonate determinations filters were fumed for two hours in air saturated hydrochloric acid (HCl) to remove inorganic carbon, and dried at 40 °C overnight. Carbon measurements were carried out as for POC determination. Particulate inorganic carbon was determined by subtracting the POC content on the fumed filters from the POC content on the non-fumed filters. The ratio of POC to DW for each of the three aggregate types was calculated by dividing the amount of POC by the DW of the material on each filter. The POC content of each aggregate was estimated by multiplying the DW of the aggregate by the POC:DW ratio for that aggregate type.

2.7 Density of aggregates

We used the Navier-Stokes drag equation to calculate the excess density ($\Delta\rho$) of our aggregates (Stokes, 1851):

$$\Delta\rho = \frac{C_D \rho_w w^2}{\frac{4}{3} g \mathrm{ESD}} \quad (1)$$

where C_D is the dimensionless drag force defined in Eq. (3), ρ_w is the density of sea water ($1.0237\,g\,cm^{-3}$, at 15 °C and salinity of 32), w is the measured sinking velocity in $cm\,s^{-1}$, g is the gravitational acceleration of $981\,cm\,s^{-2}$, and ESD is the equivalent spherical diameter in cm. We calculated C_D using the drag equation for $Re > 1$ given by White (1974):

$$C_D = \left(\frac{24}{Re}\right) + \left(\frac{6}{1+Re^{0.5}}\right) + 0.4 \quad (2)$$

where Reynolds number (Re) was defined as:

$$Re = w\mathrm{ESD}\frac{\rho_w}{\eta} \quad (3)$$

where η is the dynamic viscosity ($1.22\times10^{-2}\,g\,cm^{-1}\,s^{-1}$, at 15 °C and salinity of 32).

3 Results

3.1 Aggregate formation

Initial cell concentrations in the roller tanks were 2×10^5 mL^{-1} for *S.c.*-inc, 4×10^5 mL^{-1} for *E.h.*-inc. In mix-inc initial cell concentrations were 1×10^5 *S. costatum* mL^{-1} and 2×10^5 *E. huxleyi* mL^{-1}. Hence, the cell ratio of *E. huxleyi* to *S. costatum* in mix-inc was 1:2. Both mix-inc and *S.c.*-inc formed aggregates within the first 24 h of incubation. *E.h.*-inc did not form aggregates until the fifth day of incubation in the roller tanks. The formation of aggregates in *E.h.*-inc started to occur when individual coccoliths rather than whole cells began to dominate the particle abundances in the tanks. The aggregates in mix-inc were dominated by diatom cells throughout the study despite higher *E. huxleyi* abundance in the tanks (Table 1). With increased incubation period both the total and relative abundance of coccoliths increased within the aggregates formed in the mix-inc incubations (Table 1). Aggregates contained individual coccoliths in both *E.h.*-inc (Fig. 1a) and mix-inc (Fig. 1b) incubations. Further, we did not observe aggregation of whole coccolithophorid cells. In mix-inc, the coccoliths seemed to be scavenged by rapidly formed diatom aggregates. This may explain the increasing abundance of coccoliths relative to diatoms within the aggregates over time (Table 1). The aggregates formed in *E.h.*-inc were in general smaller and more spherical than the aggregate in *S.c.*-inc and mix-inc (Table 2).

3.2 Aggregate dry weight

The DW increased with increasing aggregate size for all three aggregate types (Fig. 2). Size-specific aggregate DW varied more in aggregates containing *S. costatum* (large, chain-forming diatom) as compared to those formed by small *E. huxleyi* coccoliths (Fig. 2). Hence, the correlation coefficients between DW and aggregate size were higher for *E.h.*-inc as compared to those for *S.c.*-inc and mix-inc, indicating more uniform aggregate structures when formed solely from *E. huxleyi* (Fig. 2b). Power regressions were chosen due to the fractal nature of the aggregates. The more uniform structure of the *E.h.*-inc aggregates may be due to the small size of the constituting particles (coccoliths) within the aggregates, resulting in compact and relative small aggregates compared to aggregates formed from *S.c.*-inc and mix-inc (Fig. 1). In mix-inc (Fig. 2c), a variety of aggregate structures were formed, depending on the ratio of coccolith to diatom cells (Table 1), which resulted in no apparent relationship between DW and aggregate size as reflected by the ESD.

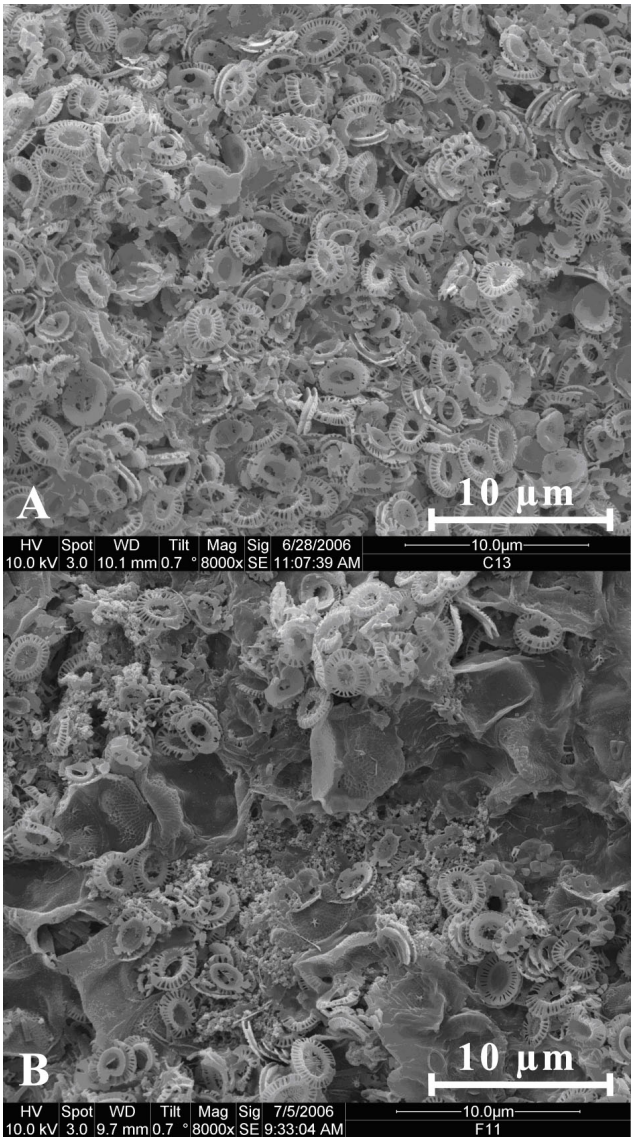

Fig. 1. *Scanning electron microscopic (SEM) images*. **(A)** aggregates formed from *E. huxleyi* and **(B)** aggregates formed from a mix of *Skeletonema costatum* and *Emiliania huxleyi*. Only single *E. huxleyi* coccoliths are observed in aggregates. *S. costatum* dominated in the aggregates formed in the mixed incubation (B).

3.3 Aggregate sinking velocity

Sinking velocity increased with increasing aggregate size in all three types of aggregates (Fig. 3a). Aggregates formed from *E.h.*-inc showed about 2-fold and 2.5-fold higher size-specific sinking velocities than aggregates formed by mix-inc and *S.c.*-inc, respectively (Fig. 3a). The largest variability in size-specific sinking velocities was observed for the aggregates formed from the mix-inc (Fig. 3a). The presence of coccoliths within these aggregates enhanced their sinking velocities as compared to those of similarly-sized pure diatom aggregates.

Table 1. Temporal evolution of aggregate composition given in number of *S. costatum* and *E. huxleyi* coccoliths per unit volume of aggregate in the mix-inc incubation.

Incubation time (days)	*S. costatum* (cells mm^{-3})	*E. huxleyi* (liths mm^{-3})	*E.h*: *S.c* Ratio	Aggregate volume (mm^3)
2	66,297	1146	1:60	6.98
5	91,398	3763	1:25	5.58
6	139,263	5598	1:25	3.26

3.4 Aggregate excess density

The excess densities derived from aggregate sinking velocity and sizes are shown in Fig. 3b. Due to the fractal nature of the aggregates, their excess densities decrease with increasing size, i.e., their porosity increases with increasing aggregate size. The excess densities were on average 2- to 3-fold higher for aggregates formed by *E.h.*-inc as compared to those of the other aggregate types. Aggregates formed in mix-inc had 1.4-fold higher excess densities as compared to those formed in *S.c.*-inc (Fig. 3b).

3.5 Particulate organic carbon content and respiration rate

Particulate organic carbon (POC) content in the aggregates increased with increasing aggregate size (Fig. 4a). POC comprised ∼24% of the dry weight in the aggregates formed in *S.c.*-inc, and ∼22% of the dry weight in the other two aggregate types. No significant differences were found for the POC content between the different aggregate types (p = 0.133, One Way ANOVA). The inorganic carbon to POC ratio was 0.08 ± 0.005, 0.14 ± 0.09, and 0.24 ± 0.01 for the aggregates formed in *S.c.*-inc, mix-inc, and *E.h.*-inc, respectively. The respiration rate per aggregate increased with increasing aggregate size, and was relatively similar in small aggregates (<3 mm) of different types (Fig. 4b). Respiration rate increased proportional to POC content of the aggregates, indicating first-order kinetics of POC degradation (Fig. 4c). However, some scatter is observed which might be due to the use of a constant POC:DW ratio for each aggregate type used to estimate the POC content in each aggregate across the size spectra. The carbon-specific respiration rate was calculated by dividing the carbon respiration rate with the total POC content of each aggregate. The average carbon-specific respiration rate was ∼0.13 d^{-1} (Table 2), and showed no significant differences between the three types of aggregates ($p > 0.67$, Students t-test). However, a large variability was observed for the carbon-specific respiration rates in all types of aggregates (Fig. 4d). The apparent size-dependency of the carbon-specific respiration rate for the aggregates formed in *E.h.*-inc was likely due to the scarcity of measurements for large aggregates (two measurements of aggregates >3mm) (Fig. 4d). Hence, all three types of aggregates appeared to have size-independent carbon-specific respiration rates.

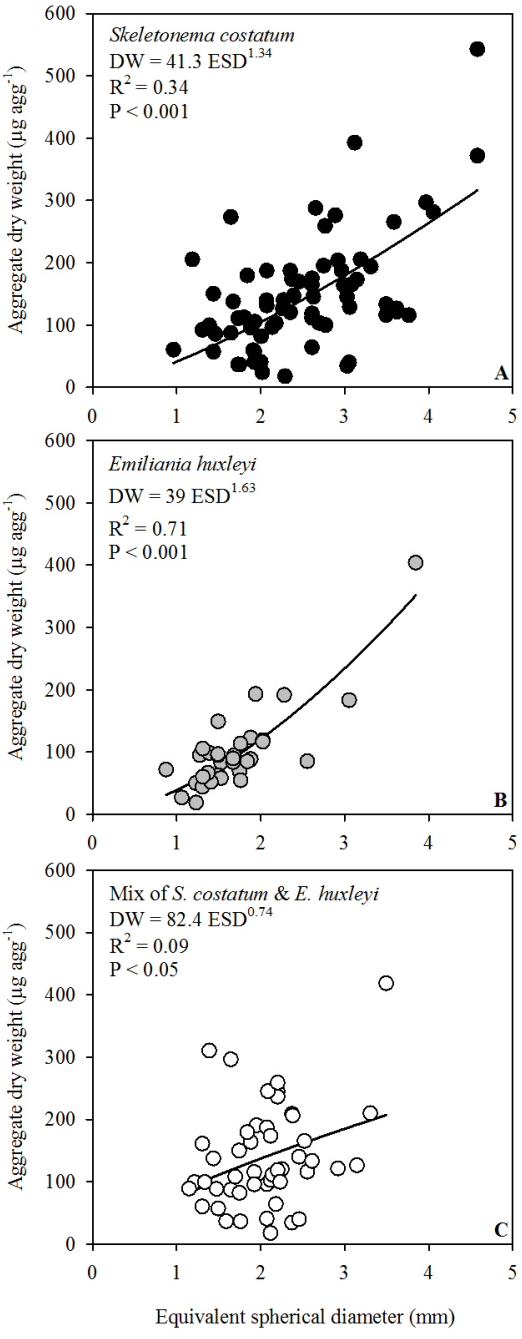

Fig. 2. *Aggregate dry weight as a function of aggregate size* for the three different incubation experimentst: **(A)** *Skeletonema costatum* (black circles), **(B)** *Emiliania huxleyi* (grey circles), and **(C)** Mixed culture of *S. costatum* and *E. huxleyi* (open circles). Regressions curves between measured dry weights and sizes are showed as solid lines in each plot. Regression curves and the correlation coefficients (R^2) are given in each plot.

Table 2. Source and incubation treatment, sample size, averages, and standard deviations of aggregate size (Agg size), carbon-specific respiration rate (C-spec. resp.), sinking velocity, and ratio of L for the three types of aggregates investigated.

Source	No. in sample	Agg size (mm)	C-spec. resp. (d^{-1})	Settling velocity ($m\,d^{-1}$)	L ($\times 10^{-4}\,m^{-1}$)
S. costatum (*S.c.*-inc)	26	2.51 ± 0.83	0.13 ± 0.09	113 ± 42	13.1 ± 5.0
E. huxleyi (*E.h.*-inc)	12	1.67 ± 0.68	0.13 ± 0.13	246 ± 41	5.5 ± 0.9
Mix of *S. costatum* and *E. huxleyi* (mix-inc)	24	2.02 ± 0.48	0.12 ± 0.07	125 ± 26	10.4 ± 2.7

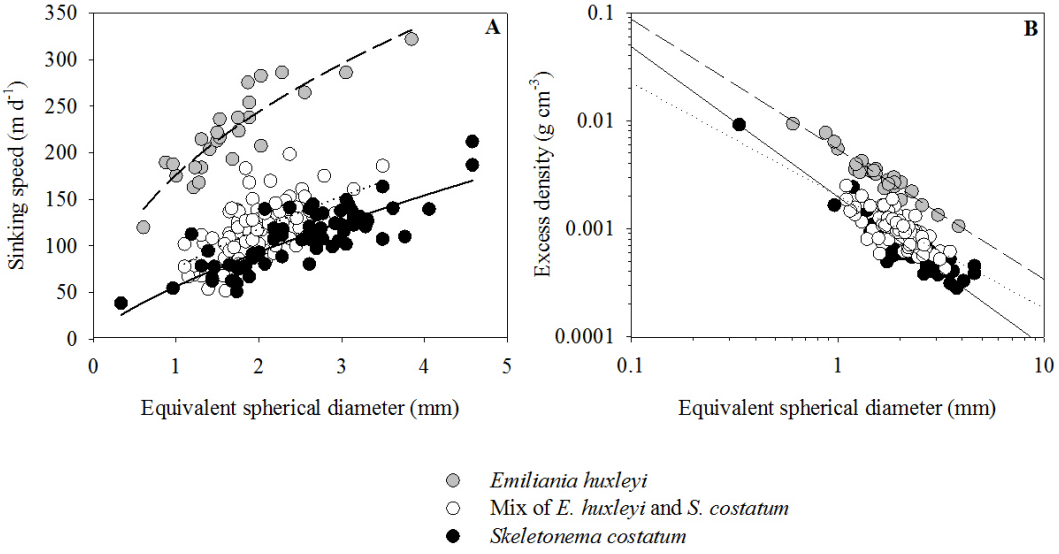

Fig. 3. *Aggregate sinking velocity and excess density*. Sinking velocity **(A)** and excess density **(B)** as a function of equivalent spherical diameter (ESD). Black circles are aggregates formed from *Skeletonema costatum* (*S.c.*-inc), grey circles are aggregates formed from *Emiliania huxleyi* (*E.h.*-inc), and open circles are aggregates formed from a mix of *S. costatum* and *E. huxleyi* (mix-inc). (A) Relationship between sinking velocities (SV) and ESD is modeled using a power law curve fitted to the data: SV = 56.56 $ESD^{0.72}$, ($R^2 = 0.65$) for the aggregates formed from diatoms (solid line). SV = 75.79 $ESD^{0.64}$, ($R^2 = 0.38$) for the aggregates formed from a mix of diatoms and *E. huxleyi* (dotted line). SV = 176.3 $ESD^{0.47}$, ($R^2 = 0.80$) for the aggregates formed from *E. huxleyi* (dashed line). (B) Relationship between excess densities ($\Delta\rho$) and ESD is modeled using a power law curve fitted to the data: $\Delta\rho$ = 0.005 $ESD^{-1.21}$, ($R^2 = 0.94$) for the aggregates formed from diatoms (solid line). $\Delta\rho$ = 0.002 $ESD^{-1.05}$, ($R^2 = 0.52$) for the aggregates formed from a mix of diatoms and *E. huxleyi* (dotted line). $\Delta\rho$ = 0.002 $ESD^{-1.39}$, ($R^2 = 0.97$) for the aggregates formed from *E. huxleyi* (dashed line).

3.6 Remineralization length scale of aggregates

The remineralization length scale, L (m^{-1}), is calculated by dividing the carbon-specific respiration rate by the settling velocity of the aggregates, and it expresses the fractional remineralization in aggregates per m settled. L decreased with increasing aggregate size for all aggregate types (Fig. 4e). The higher sinking velocity of aggregates formed from *E.h.*-inc compared to the two other aggregate types resulted in lower L in *E.h.*-inc aggregates, both when considering size-specific values (Fig. 4e) and when averaged across the aggregate size spectrum (Table 2). The remineralization length scale of large aggregates formed by mix-inc was closer to that of *E.h.*-inc than to *S.c.*-inc (Fig. 4e). This was due to the slightly higher ballasting effect of coccoliths in mix-inc compared to *S.c.*-inc (Fig. 3b) leading to higher size-specific sinking velocities of the large mix-inc aggregates.

4 Discussion

Collision of particles and aggregate formation is driven by wind-induced shear and differential settling of particles in the ocean (Jackson, 1990; Kiørboe et al., 1990).

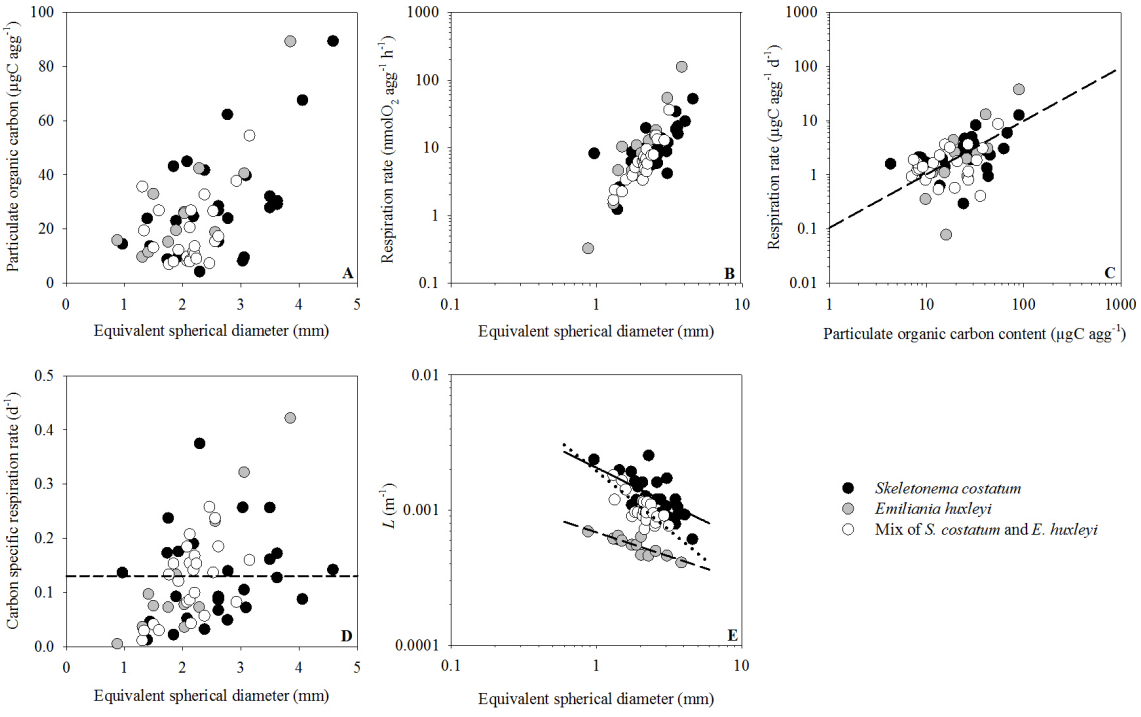

Fig. 4. *Size and carbon-specific parameters of aggregates*. All measurements were done on three different aggregate types formed from (1) incubation with *Skeletonema costatum* (black circles), (2) incubation with *Emiliania huxleyi* (grey circles), and (3) incubation of a mix of both *S. costatum* and *E. huxleyi* (open circles). **(A)** Aggregate particulate organic carbon (POC) content (μgC agg^{-1}) as a function of equivalent spherical diameter (ESD in mm). **(B)** Microbial respiration rate (nmolO_2 agg^{-1} h^{-1}) as a function of ESD. **(C)** Respiration rate (μgC agg^{-1} d^{-1}) as a function of POC content. The regression curve is based on a power law relationship with: Respiration rate = 0.11 POC$^{0.99}$, ($R^2 = 0.43$). **(D)** Carbon specific respiration rate (d^{-1}) as a function of ESD. The dashed line indicates the average carbon-specific respiration rate of 0.13 d^{-1}. **(E)** Remineralization length scale L (m^{-1}) as a function of ESD. The regression curves are based on a power law relationship with L = 0.0021 ESD$^{0.53}$ ($R^2 = 0.3$) for $E.h.$-inc (solid line). L = 0.0019 ESD$^{0.87}$ ($R^2 = 0.60$) for mix-inc (dotted line) and L = 0.0007 ESD$^{0.36}$ ($R^2 = 0.78$) for $S.c.$-inc (dashed line).

Table 3. Carbon specific respiration rates (C-resp.) of aggregates (agg) and copepod fecal pellets (pellets) of different type, composition, and origin from five different studies. F-max indicates aggregates formed from water collected at the depth of fluorescence maximum off Cape Blanc.

Aggregate type	C-resp. (d^{-1})	Reference
F-max water Cape Blanc, NW Africa (agg)	0.13 ± 0.07	Iversen et al., 2010
S. costatum (agg)	0.13 ± 0.09	Present study
E. huxleyi (agg)	0.13 ± 0.13	Present study
Mix of *S. costatum and E. huxleyi* (agg)	0.12 ± 0.07	Present study
Rhodomonas sp. (pellets)	0.16	Ploug et al., 2008b
T. weissflogii (pellets)	0.20	Ploug et al., 2008b
T. weissflogii (pellets)	0.12	Ploug et al., 2008b
E. huxleyi (pellets)	0.21	Ploug et al., 2008b
E. huxleyi (pellets)	0.08	Ploug et al., 2008b
*Diatoms + natural community (agg)	0.08 ± 0.03	Ploug and Grossart, 2000
In situ collected marine snow (California)	0.10 to 0.12	Ploug et al., 1999

* Diatom cultures incubated with filtered (80 µm mesh size) Baltic Sea water.

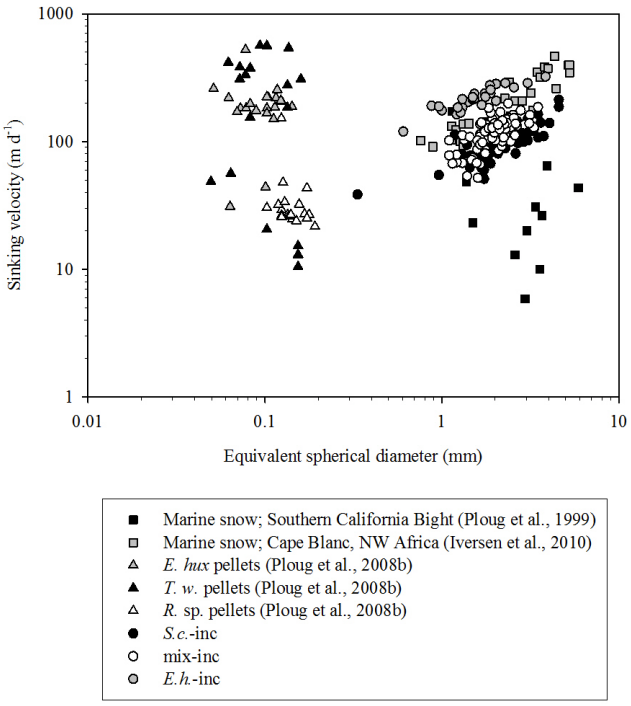

Fig. 5. Sinking velocity as a function of aggregate size for a wide range of fecal pellets, marine snow, and phytoplankton-derived aggregates. The *E. hux*, $T.w.$, and $R.$ sp pellets are copepod fecal pellet produced by *Temora longicornis* feeding on *Emiliania huxleyi*, *Thalassiosira wiessflogii*, and *Rhodomonas* sp., respectively (Ploug et al., 2008b).

The stickiness of particles determines if coagulation occurs (Hill, 1992; Riebesell and Wolf-Gladrow, 1992; Kiørboe and Hansen, 1993). The dominant process leading to collision in roller tanks is differential settling (Shanks and Edmondson, 1989). Diatoms often form chains consisting of many cells, e.g. *S. costatum* as used in the present study, and tend to be very sticky (Kiørboe et al., 1990) due to their production of transparent exopolymer particles (TEP) (Alldredge et al., 1993; Kiørboe and Hansen, 1993). Hence, their large size and stickiness explain the fast aggregate formation observed in the two incubations containing diatoms, $S.c.$-inc and mix-inc. In contrast, aggregate formation took much longer in $E.h.$-inc. The first aggregate formations in $E.h.$-inc co-occurred with the release of single coccoliths. The occurrence of single coccoliths may be due to cell lysis of *E. huxleyi* after being kept in the dark for five days. Cell lysis of *E. huxleyi* often occurs in situ due to viral attack, leading to bloom termination (Bratbak et al., 1993; Brussaard et al., 1996; Wilson et al., 2002). In addition, cell lysis can also increase the concentration of dissolved organic carbon (DOC) (Fuhrman, 1999). Suboptimal growth conditions also leads to exudation of DOC (mainly polysaccharides) in phytoplankton (e.g. Mari and Burd, 1998). DOC can be adsorbed on coccolith surfaces (Engel et al., 2009a) and promote coagulation by increasing coccoltih stickiness. Increasing concentrations of released DOC, in the present study, probably induced coccolith coagulation after five days of incubation when the first aggregates were observed in $E.h.$-inc. Adsorption of DOC on the coccolith surfaces might also explain why the aggregates formed from coccoliths had POC to dry weight ratios similar to aggregates containing whole diatom cells.

Blooms of *E. huxleyi* can cover large areas and reach high cell concentration in the ocean (Robertson et al., 1994). However, presence of aggregates constituted exclusively of coccolith or coccolithophore has never been observed in the field (De La Rocha and Passow, 2007). Coccolithophores and coccoliths mainly seem transported to depths in situ via scavenging by gelatinous aggregates (Honjo, 1982) and marine snow aggregates (Iversen et al., 2010) or packed within zooplankton fecal pellets (Knappertsbusch and Brummer, 1995; Ploug et al., 2008a). Engel et al. (2004) observed aggregation of *E. huxleyi* into marine snow during a mesocosm bloom study. Calcified coccolithophore aggregates showed low scavenging efficiencies (Engel et al., 2009b) with 1-2 orders of magnitude lower efficiencies in calcified compared to non-calcified coccolithophores. Thus, high cell concentrations ($\sim 4 \times 10^5$ cell mL^{-1}) are needed for the formation of large coccolithophore aggregates. Such conditions occurred in the present study. Natural blooms of *E. huxleyi* can also reach similar cell densities (Robertson et al., 1994). However, aggregation may not occur until the end-bloom where nutrient depletion leads to large release of DOC. The present and previous studies (Engel et al., 2004; Engel et al., 2009a; Engel et al., 2009b) show that aggregates can still form from coccoliths and/or coccolithophores at high cell concentrations.

Aggregates with coccoliths were more compact and had higher excess densities than those containing diatoms. TEPs occupy a significant fraction of aggregate volume but contribute little to DW in diatom aggregates (Ploug and Passow, 2007). TEP densities can be lower than that of seawater and decrease aggregate sinking velocities (Engel and Schartau, 1999; Azetsu-Scott and Passow, 2004). The porosity of *E. huxleyi* aggregates has been shown to be ~96% and that of *S. costatum* aggregates to be ~99% (Ploug et al. 2008a). Hence, *E. huxleyi* aggregates were more compact than aggregates with *S. costatum* (Ploug et al., 2008a). The higher excess densities of aggregates containing coccoliths may also partly be explained by the 1.3-fold higher density of biogenic calcite (2.7 g cm^{-3}) compared to that of biogenic opal (2.09 g cm^{-3}). These factors can explain the higher size-specific settling velocities of aggregates formed from $E.h.$-inc compared to those of the other two treatments (Fig. 3). Engel et al. (2009b) also suggested lower drag forces on aggregates formed from calcified compared to non-calcified coccolithophorids due to the spherical and compact nature of calcified coccolithophorid aggregates. We also observed aggregates formed from $E.h.$-inc to be more spherical than the

other two aggregate types, indicating that lower drag forces may contribute to the higher sinking velocities of *E.h.*-inc aggregates.

Previous studies of diatom aggregates mixed with minerals, e.g., clays and carbonate, have demonstrated that, on average, these aggregates are smaller than those formed in pure diatom cultures (Hamm, 2002; Passow and De La Rocha, 2006). In those studies, however, sinking velocity was not directly measured, but applying Stoke's law it was argued that the smaller size of mixed aggregates may lead to lower sinking velocities despite their higher content of ballasting minerals as compared to those composed of diatoms, only. In our study, the average size of aggregates formed by mix-inc was also on average smaller than that of aggregates formed by the pure diatom culture but with higher size-specific sinking velocities and excess densities. Hence, our results confirm, that sinking velocities of aggregates depend on aggregate composition and density rather than on size only, as also previously found (Ploug et al., 2008a).

Sinking velocities of similar-sized marine snow vary greatly across the aggregate size spectrum. We compiled sinking velocities that we have measured in aggregates, fecal pellets, and marine snow in the laboratory (Fig. 5). Small zooplankton fecal pellets produced on a diet of diatoms or coccolithophorids showed sinking velocities comparable to those of much larger marine snow and phytoplankton-derived aggregates as also observed in the field (Armstrong et al., 2009). Hence, small particles and aggregates do not necessarily sink slower than larger ones do when compared across different sources. The size effect on sinking velocities of mm-large particles is apparent only when comparing particles for similar composition and type.

The measurements of sinking velocities in laboratories are maximum sinking velocities. Aggregates have potentially much longer residence times in the upper ocean than those predicted by sinking velocity measurements alone (Alldredge and Gotschalk, 1988) due to turbulence, water density differences (MacIntyre et al., 1995), and zooplankton activity (Dilling and Alldredge, 2000). Sinking velocities appear to increase with increasing depth in the ocean (Berelson, 2002; Fischer and Karakas, 2009). However, a recent study found no strong evidence for increasing sinking velocity with depth when using fluxes of mass and chemical tracers to determine the most likely average sinking velocity of particles at different depths (Xue and Armstrong, 2009). During aging, the excess density and sinking velocity of diatom aggregates increase (Ploug et al., 2008a). This may be caused by the observed decrease in organic carbon to dry mass ratio in aging aggregates likely due to microbial degradation of TEP (Ploug and Passow, 2007). Hence, the sinking velocities of aggregates in the field might depend on source, density, and age rather than aggregate size (Ploug et al., 2008a). Thus, aggregates with high content of minerals and low amounts of relatively buoyant organic matter are likely to have higher size-specific sinking velocities. Such aggregates are likely to be found in the deep ocean where they had longer time for scavenging of ballast minerals and for microbial degradation compared to surface aggregates. Biominerals and lithogenic material are, therefore, important factors influencing aggregate sinking velocity and, potentially, vertical carbon fluxes in the ocean (Ploug et al., 2008a, b). This has important consequences for the paleoclimate and future climate scenarios. Increased desertification and droughts in the future could lead to higher dust availability in atmosphere and ocean (e.g. Prospero and Nees, 1976) and, hence, increased ballasting of aggregates. The higher dust load of the glacial atmosphere might also influence the marine carbon cycle via ballasting (e.g. Ittekkot, 1993).

Microbial degradation of marine snow in the ocean is largely controlled by ecto-enzymatic hydrolysis and respiration (Smith et al., 1992; Ploug et al., 1999; Ploug and Grossart, 2000). Size-specific respiration rate in the aggregates of the present study was on average proportional to particulate organic carbon content in aggregates as also found in previous studies (Ploug et al., 1999; Ploug and Grossart, 2000). As a consequence, no size dependency was observed for the carbon-specific respiration rates of the different aggregate types. Carbon-specific respiration rates for the aggregates shown in Fig. 5 are compiled in Table 3. The average carbon-specific respiration rates measured in the present study are within the range of previous measurements for zooplankton fecal pellets (Ploug et al., 2008b), marine snow (Ploug et al., 1999), and aggregates formed from diatom detritus incubated with natural microbial communities from the Baltic Sea (Ploug and Grossart, 2000) as well as aggregates formed from organic matter sampled off Cape Blanc, NW Africa (Iversen et al., 2010) (Table 3). Thus, it appears that carbon-specific respiration rates are relatively similar across different types of marine particles irrespective of composition, size, and type. The apparent diffusivities of solutes and oxygen supply for respiration were high for all particle types supporting an efficient turnover of organic carbon (Ploug et al., 2008a). However, these rates presumably only apply to the upper ocean, since they were measured within relatively fresh particles with high organic carbon content. The comparable carbon-specific remineralization rates over such a wide range of particle types and sizes indicate that carbon remineralization in the upper ocean is to a large extent controlled by residence times of aggregates in the water column. The residence time of aggregates depends on physical (e.g., turbulence, sinking velocity, fractionation by swimming zooplankton) as well as on biological processes (e.g., ecto-enzymatic hydrolysis, microbial respiration, feeding by zooplankton) in the upper ocean, whereas microbial respiration and sinking velocity dominates at increasing depth where zooplankton are scare and turbulence is low (Iversen et al., 2010). Our results show that ballasting of aggregates in the upper ocean appears to have a large influence on sinking velocities, while the similar average carbon-specific respiration rates between the treatments indicate no protective

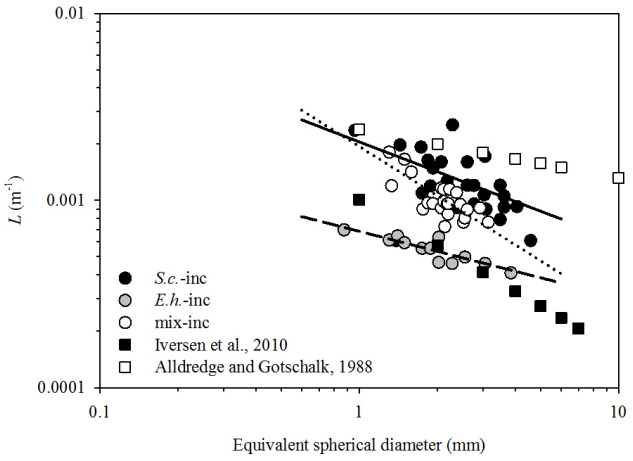

Fig. 6. Remineralization length scale (L) as a function of aggregate size for aggregates investigated in the present study ($S.c.$-inc, $E.h.$-inc and mix-inc), calculated for aggregates from a diatom dominated area (Alldredge and Gotschalk, 1988) and for aggregates formed from in situ material collected in a carbonate dominated area (Iversen et al., 2010) using the sinking velocities found in Alldredge and Gotschalk (1988) and the carbon-specific respiration rate found by Ploug et al. (1999). Regression lines are the same as in Fig. 4e.

mechanisms against remineralization of labile organic matter as also found in copepod fecal pellets (Ploug et al., 2008b). Further the remineralization length scale of our aggregates was similar to those of opal- and carbonate-ballasted copepod fecal pellets (Ploug et al., 2008b). Finally, carbonate-ballasted aggregates are potentially more efficient for carbon export from the upper ocean as compared to aggregates only ballasted by opal as also suggested by recent studies (Francois et al., 2002; Klaas and Archer, 2002; Lee et al., 2009). Estimates of the remineralization length scale (L) for aggregates from an opal dominated area off California using a carbon-specific respiration rate of $0.10\,d^{-1}$ (Ploug et al., 1999) and the size-specific sinking velocities measured in situ by Alldredge and Gotschalk (1988) shows that our laboratory results are similar to those predicted in the field. Furthermore, aggregates ballasted by carbonate and lithogenic material, formed by a heterogeneous pool of organic and inorganic material collected in the field (Iversen et al., 2010), show sinking velocities similar to aggregates from $E.h.$-inc in the present study (Fig. 6). This further supports the notion that ballasting by carbonate and lithogenic material may indeed enhance vertical carbon export as compared to opal ballasting (Francois et al., 2002; Klaas and Archer, 2002).

Acknowledgements. We thank Christiane Lorenzen for assistance during POC measurements. The oxygen microelectrodes were constructed by Gaby Eickert, Ines Schröder, and Karin Hohmann, Max Planck Institute for Marine Microbiology, Bremen. We thank Uta Passow and Gerhard Fischer for discussions and Christine Klaas and two anonymous reviewers for critical comments that improved the manuscript. This study was supported by the Helmholtz Association (to HP), the Alfred Wegener Institute for Polar and Marine Research (to MHI and HP), and by the DFG-Research Center/Cluster of Excellence "The Ocean in the Earth System" (to MHI and HP).

Edited by: E. Boss

References

Alldredge, A. and Gotschalk, C.: *In situ* settling behavior of marine snow, Limnol. Oceanogr., 33, 339–351, 1988.

Alldredge, A. L. and Silver, M. W.: Characteristics, dynamics and significance of marine snow, Prog. Oceanogr., 20, 41–82, 1988.

Alldredge, A. L., Passow, U., and Logan, B. E.: The abundance and significance of a class of large, transparent organic particles in the ocean, Deep-Sea Res. Pt. I, 40, 1131–1140, 1993.

Armstrong, R. A., Lee, C., Hedges, J. I., Honjo, S., and Wakeham, S. G.: A new, mechanistic model for organic carbon fluxes in the ocean based on the quantitative association of POC with ballast minerals, Deep-Sea Res. Pt. II, 49, 219–236, 2002.

Armstrong, R. A., Peterson, M. L., Lee, C., and Wakeham, S. G.: Settling velocity spectra and the ballast ratio hypothesis, Deep-Sea Res. Pt. II, 56, 1470–1478, 2009.

Azetsu-Scott, K. and Passow, U.: Ascending marine particles: Significance of transparent exopolymer particles (TEP) in the upper ocean, Limnol. Oceanogr., 49, 741–748, 2004.

Berelson, W. M.: Particle settling rates increase with depth on the ocean, Deep-Sea Res. Pt. II, 49, 237–251, 2002.

Bratbak, G., Egge, J. K., and Heldal, M.: Viral mortality of the marine alga *Emiliania huxleyi* (Haptophyceae) and termination of algal blooms, Mar. Ecol. Prog. Ser, 93, 39–48, 1993.

Broecker, W. S. and Peng, T. H.: Gas exchange rates between air and sea, Tellus, 26, 21–35, 1974.

Brussaard, C. D. P., Kempers, R. S., Kop, A. J., Riegman, R., and Heldal, M.: Virus like particles in a summer bloom of *Emiliania huxleyi* in the North Sea, Aquat. Microb. Ecol., 10, 105–113, 1996.

De La Rocha, C. L. and Passow, U.: Factors influencing the sinking of POC and the efficiency of the biological carbon pump, Deep-Sea Res. Pt. II, 54, 639–658, 2007.

De La Rocha, C. L., Nowald, N., and Passow, U.: Interactions between diatom aggregates, minerals, particulate organic carbon, and dissolved organic matter: Further implications for the ballast hypothesis, Global Biogeochem. Cycles, 22, GB4005, doi:10.1029/2007GB003156, 2008.

Dilling, L. and Alldredge, A. L.: Fragmentation of marine snow by swimming macrozooplankton: A new process impacting carbon cycling in the sea, Deep-Sea Res. Pt. I, 47, 1227–1245, 2000.

Engel, A. and Schartau, M.: Influence of transparent exopolymer particles (TEP) on sinking velocity of Nitzschia closterium aggregates, Mar. Ecol. Prog. Ser., 182, 69–76, 1999.

Engel, A., Delille, B., Jacquet, S., Riebesell, U., Rochelle-Newall, E., Terbrueggen, A., and Zondervan, I.: Transparent exopolymer particles and dissolved organic carbon production by *Emiliania huxleyi* exposed to different CO_2 concentrations: a mesocosm experiment, Aquat. Microb. Ecol., 34, 93–104, 2004.

Engel, A., Abramson, L., Szlosek, J., Liu, Z., Steward, G., Hirschberg, D., and Lee, C.: Investigating the effect of ballasting by $CaCO_3$ in *Emiliania huxleyi*, II: Decomposition of particulate organic matter, Deep-Sea Res. Pt. II, 56, 1408–1419, 2009a.

Engel, A., Szlosek, J., Abramson, L., Liu, Z., and Lee, C.: Investigating the effect of ballasting by $CaCO_3$ in *Emiliania huxleyi*: I. Formation, settling velocities and physical properties of aggregates, Deep-Sea Res. Pt. II, 56, 1396–1407, 2009b.

Fischer, G. and Karakas,, G.: Sinking rates and ballast composition of particles in the Atlantic Ocean: implications for the organic carbon fluxes to the deep ocean, Biogeosciences, 6, 85–102, doi:10.5194/bg-6-85-2009, 2009.

Francois, R., Honjo, S., Krishfield, R., and Manganini, S.: Factors controlling the flux of organic carbon to the bathypelagic zone of the ocean, Global Biogeochem. Cy., 16(4), 1087, doi:10.1029/2001GB001722, 2002.

Fuhrman, J. A.: Marine viruses and their biogeochemical and ecological effects, Nature, 3999, 541–548, 1999.

Guillard, R. L.: Culture of phytoplankton for feeding marine invertebrates, in: Culture of marine invertebrate animals, edited by: Smith, W., L. and Chanley, M., H., Plenum Press, New York, London, 29–60, 1975.

Hamm, C. E.: Interactive aggregation and sedimentation of diatoms and clay-sized lithogenic material, Limnol. Oceanogr., 47, 1790–1795, 2002.

Hill, P. S.: Reconciling aggregation theory with observed vertical fluxes following phytoplankton blooms, J. Geophys. Res., 97, 2295–2308, 1992.

Honjo, S.: Seasonality and interaction of biogenic and lithogenic particulate flux at the Panama Basin, Science, 218, 883–884, 1982.

Ittekkot, V.: The abiotically driven biological pump in the ocean and short-term fluctuations in atmospheric CO_2 contents, Global Planet. Change, 8, 17–25, 1993.

Iversen, M. H., Nowald, N., Ploug, H., Jackson, G. A., and Fischer, G.: High resolution profiles of vertical particulate organic matter export off Cape Blanc, Mauritania: Degradation processes and ballasting effects, Deep-Sea Res. Pt. I, 771–784, doi:10.1016/j.dsr.2010.1003.1007, 2010.

Jackson, G. A.: A model of the formation of marine algal flocs by physical coagulation processes, Deep-Sea Res., 37, 1197–1211, 1990.

Kiørboe, T., Andersen, K. P., and Dam, H. G.: Coagulation efficiency and aggregate formation in marine phytoplankton, Mar. Biol., 107, 235–245, 1990.

Kiørboe, T. and Hansen, J. L. S.: Phytoplankton aggregate formation: Observations of patterns and mechanisms of cell sticking and the significance of exopolymeric material, J. Plankton Res., 15, 993–1018, 1993.

Kiørboe, T., Ploug, H., and Thygesen, U. H.: Fluid motion and solute distribution around sinking aggregates. I. Small-scale fluxes and heterogeneity of nutrients in the pelagic environment, Mar. Ecol. Prog. Ser., 211, 1–13, 2001.

Klaas, C. and Archer, D. E.: Association of sinking organic matter with various types of mineral ballast in the deep sea; implications for the rain ratio, Global Biogeochem. Cy., 16(4), 1–13, 1116, doi:10.1029/2001GB001765, 2002.

Knappertsbusch, M. and Brummer, G. J. A.: A sediment trap investigation of sinking coccolithophorids in the North Atlantic, Deep-Sea Res. Pt. I, 42, 1083–1109, 1995.

Lee, C., Peterson, M. L., Wakeham, S. G., Armstrong, R. A., Cochran, J. K., Miquel, J. C., Fowler, S. W., Hirschberg, D., Beck, A., and Xue, J.: Particulate organic matter and ballast fluxes measured using time-series and settling velocity sediment traps in the northwestern Mediterranean Sea, Deep-Sea Res. Pt. II, 56, 1420–1436, 2009.

Maas, L. R. M.: On the surface area of an ellipsoid and related integrals of elliptic integrals., J. Comp. Appl. Math., 51, 237–249, 1994.

MacIntyre, S., Alldredge, A. L., and Gotschalk, C. C.: Accumulation of marine snow at density discontinuities in the water column, Limnol. Oceanogr., 40, 449–468, 1995.

Mari, X. and Burd, A.: Seasonal size spectra of transparent exopolymeric particles (TEP) in a coastal sea and comparison with those predicted using coagulation theory, Mar. Ecol. Prog. Ser., 163, 63–76, 1998.

Passow, U. and De La Rocha, C.: Accumulation of mineral ballast on organic aggregates, Global Biogeochem. Cy., 20, 1–7, 2006.

Ploug, H., Kuehl, M., Buchholz-Cleven, B., and Jørgensen, B. B.: Anoxic aggregates - An ephemeral phenomenon in the pelagic environment?, Aquat. Microb. Ecol., 13, 285–294, 1997.

Ploug, H., Grossart, H. P., Azam, F., and Jørgensen, B. B.: Photosynthesis, respiration, and carbon turnover in sinking marine snow from surface waters of Southern California Bight: Implications for the carbon cycle in the ocean, Mar. Ecol. Prog. Ser., 179, 1–11, 1999.

Ploug, H. and Jørgensen, B. B.: A net-jet flow system for mass transfer and microsensor studies of sinking aggregates, Mar. Ecol. Prog. Ser., 176, 279–290, 1999.

Ploug, H. and Grossart, H. P.: Bacterial growth and grazing on diatom aggregates: Respiratory carbon turnover as a function of aggregate size and sinking velocity, Limnol. Oceanogr., 45, 1467–1475, 2000.

Ploug, H. and Passow, U.: Direct measurement of diffusivity within diatom aggregates containing transparent exopolymer particles, Limnol. Oceanogr., 52, 1–6, 2007.

Ploug, H., Iversen, M. H., and Fischer, G.: Ballast, sinking velocity, and apparent diffusivity within marine snow and zooplankton fecal pellets: Implications for substrate turnover by attached bacteria, Limnol. Oceanogr., 53, 1878–1886, 2008a.

Ploug, H., Iversen, M. H., Koski, M., and Buitenhuis, E. T.: Production, oxygen respiration rates, and sinking velocity of copepod fecal pellets: Direct measurements of ballasting by opal and calcite, Limnol. Oceanogr., 53, 469–476, 2008b.

Ploug, H., Terbrüggen, A., Kaufmann, A., Wolf-Gladrow, D., and Passow, U.: A novel method to measure particle sinking velocity *in vitro*, and its comparison to three other *in vitro* methods, Limnol. Oceanogr. Methods, 8, 386–393, 2010.

Prospero, J. M. and Nees, R. T.: Dust concentration in the atmosphere of the Equatorial North Atlantic: Possible relationship to the Sahelian drougth, Science, 196, 1196–1198, 1976.

Revsbech, N. P.: An oxygen microsensor with a guard cathode, Limnol. Oceanogr., 34, 474–478, 1989.

Riebesell, U. and Wolf-Gladrow, D. A.: The relationship between physical aggregation of phytoplankton and particle flux: a numerical model, Deep Sea Res., 39, 1085–1102, 1992.

Robertson, J. E., Robinson, C., Turner, D. R., Holligan, P., Watson, A. J., Boyd, P., Fernández, E., and Finch, M.: The impact of a coccolithophore bloom on oceanic carbon uptake in the northeast Atlantic during summer 1991, Deep-Sea Res. Pt. I, 41, 297–314, 1994.

Shanks, A. L. and Edmondson, E. W.: Laboratory-made artificial marine snow: A biological model of the real thing, Mar. Biol., 101, 463–470, 1989.

Smith, D. C., Simon, M., Alldredge, A. L., and Azam, F.: Intense hydrolytic enzyme activity on marine aggregates and implications for rapid particle dissolution, Nature, 359, 139–142, 1992.

Stokes, G. G.: On the effect of the internal friction of fluids on the motion of pendulums., Transaction of the Cambridge Philosophical Society, 9, 8–106, 1851.

White, F. M.: Viscous fluid flow, 2nd edition, McGraw-Hill ed., Inc. New York, New York, 1974.

Wilson, W. H., Tarran, G. A., and Zubkov, M. V.: Virus dynamics in a coccolithophore dominated bloom in the North Sea, Deep-Sea Res. Pt. I, 49, 2951–2963, 2002.

Xue, J. and Armstrong, R. A.: An improved ”benchmark” method for estimating particle settling velocities from time-series sediment trap fluxes, Deep-Sea Res. Pt. II, 56, 1479–1486, 2009.